Self-propulsion simulation of DARPA Suboff

Ali Dogrul & Savas Sezen
Yildiz Technical University, Istanbul, Turkey

Cihad Delen & Sakir Bal
Istanbul Technical University, Istanbul, Turkey

ABSTRACT: Hydrodynamic performance prediction of a propeller working behind a submerged body is a popular research field. For a submarine propeller, the propeller-hull interaction should be considered during the preliminary design stage. In this study, the resistance and propulsion analyses of the well-known benchmark DARPA Suboff with E1619 propeller have been done using Computational Fluid Dynamics (CFD) method. Self-propulsion of the submarine has been modeled with actuator disc based on body force method and with the propeller itself behind the submarine. The flow has been considered as 3-D, fully turbulent, incompressible and steady, thus the governing equations (RANSE) have been discretized with finite volume method (FVM). Uncertainty analysis has also been carried out to determine the optimum cell number in terms of total resistance. The numerical results have been compared with the available experimental data. The applicability of CFD method on self-propulsion performance prediction of the underwater vehicles has been discussed.

1 INTRODUCTION

The technology of unmanned underwater vehicles, which provide the opportunity to work in hazardous areas, are improving rapidly especially for military and research purposes. The complexity of the work being done, the variability and the difficulty of environmental conditions is gaining importance in the design phase of the vehicle (Vaz et al. 2010). The interaction between propeller and the hull of underwater vehicle is therefore very important and should be determined precisely and reliably in the preliminary design stage of unmanned vehicles.

In the past, Zhang et al. have made a study involving the interaction between propeller and a submarine hull. The analyses have been made by taking the free surface effect into account. The results show a good agreement with the experiments (Zhang et al. 2014). Berger et al. have been focused on the propeller hull interaction with a coupled method. The numerical study has been carried out for the well-known benchmark case KRISO container ship (KCS). The velocity field gathered from the RANSE solver has been given as an input to the potential solver. After the newly calculated velocity field has been applied to the RANSE solver and the flow is solved by taking the propeller hull interaction into account. The numerical results of the model propeller have been compared with those of a fully RANSE computation. By employing the propeller model with the developed code, computation time has been decreased drastically. Especially the thrust prediction has become quicker (Berger et al. 2011). Rijpkema et al. have studied the propeller-hull interaction by simulating the steady viscous flow around KCS hull with RANSE method and unsteady propeller flow with BEM. The numerical analyses have been carried out via a hybrid method. The coupled RANSE-BEM approach has given accurate results for thrust compared with the experimental data (Rijpkema et al. 2013). A comprehensive study has been made by Ozdemir et al. in order to predict resistance and wave profile of KCS numerically. The numerical method has been validated with the experimental data in terms of total ship resistance and wave profiles along the hull (Ozdemir et al. 2016). A numerical study has been conducted for resistance, propeller open water and self-propulsion performance prediction for KCS hull using a RANSE solver by Seo et al. (Seo et al. 2010). Local mesh refinements have been used in order to gain a convenient mesh structure. Sliding mesh technique has been chosen for propeller tests. Numerical results have been then compared with the existing available data. Villa et al. have made a numerical simulation of the flow around a ship with self-propulsion with RANSE solver. The coupled method solves the viscous flow around KCS hull with RANSE solver while the performance of KP505 propeller is calculated by an unsteady panel method (Villa et al.

2012). The propeller-ship interaction has been investigated by a commercial CFD program for DTC Post-Panamax Container Ship in Kinaci et al. The ship has been analyzed without taking free surface effect into account (Kinaci et al. 2013). In another study of Kinaci et al., CFD analyses have been carried out for resistance prediction of KRISO Container Ship. Experimental and numerical calculations have been performed for also a fully submerged body and a validation study has been made (Kinaci et al. 2016). The paper of Carrica et al. presents a method for self-propulsion calculation of surface ships. The method is based on controlling the propeller rotation speed (RPS) to find the self-propulsion point while reaching the target Froude number (Carrica et al. 2010). Chase has studied the self-propulsion problem of the well-known DARPA Suboff as a thesis work. A custom developed CFD solver has been employed for various advance coefficients. The effect of the turbulence has been observed via different turbulence models. The wake velocities have been compared with the experimental data for a constant advance coefficient (Chase 2012). A seven bladed INSEAN E1619 propeller has been studied in the presence of DARPA Suboff submarine model by Chase et al. The numerical analyses have been made by employing Delayed Detached Eddy Simulation (DDES) approach. The results have been compared with different turbulence models using four grids and three time steps for one advance coefficient. The results show that the present approach is applicable in self-propulsion performance prediction of submarines (Chase et al. 2013). The effect of bow and stern geometries on resistance of bared DARPA Suboff has been studied via CFD by Budak et al (Budak et al. 2016). A very recent study has been carried out by Delen et al. in order to predict the self-propulsion performance of DARPA Suboff bare hull with DTMB4119 model propeller for two different velocities (Delen et al. 2017).

In this study, resistance values and self-propulsion points of the DARPA Suboff bare form (AFF-1) have been computed. In resistance analyses, an uncertainty analysis has also been performed to identify the suitable mesh structure. Verification and validation has been made with the help of uncertainty assessment and available experimental data. The numerical results have been compared with the experiments. The suitable mesh structure has then been employed for the self-propulsion analysis. Single phase CFD analyses have been carried out for the bare hull. The flow has been considered as 3-D, fully turbulent, incompressible and steady. k-ε has been chosen as the turbulence model in the numerical calculations. Before calculation of self-propulsion point, open water results of the E1619 propeller have been computed. Two techniques have been used in self-propulsion analyses. First, a disc having the same diameter with the actual propeller has been defined in the propeller plane. The self-propulsion analysis has then been performed with actual E1619 model propeller. Self-propulsion points for both techniques have been compared with each other for DARPA Suboff bare hull for velocity, V=3.046 m/s. The applicability of the numerical method has been discussed via self-propulsion point.

2 THEORETICAL BACKGROUND

2.1 *Numerical Method*

The governing equations are the continuity equation and the well-known RANSE equations for the unsteady, three-dimensional, incompressible flow. The continuity can be given as;

$$\frac{\partial \mathrm{U_i}}{\partial \mathrm{x_i}} = 0 \tag{1}$$

Velocity U can be decomposed as mean velocity and fluctuating velocity, respectively;

$$U_i = \overline{U_i} + u_i \tag{2}$$

While the momentum equations are expressed as;

$$\frac{\partial U}{\partial t} + \frac{\partial \left(\mathrm{U_i U_j}\right)}{\partial \mathrm{x_j}} = -\frac{1}{\rho}\frac{\partial \mathrm{P}}{\partial \mathrm{x_i}} + \frac{\partial}{\partial \mathrm{x_j}}\left[\nu\left(\frac{\partial \mathrm{U_i}}{\partial \mathrm{x_j}} + \frac{\partial \mathrm{U_j}}{\partial x_i}\right)\right] - \frac{\partial \overline{\mathrm{u_i' u_j'}}}{\partial \mathrm{x_j}} \tag{3}$$

In this paper, since all simulations are run under steady state conditions, the first term in equation 3 is not taken into account. In momentum equations, $\mathrm{U_i}$ states the mean velocity while $\mathrm{u_i}$ represents the fluctuation velocity components in the direction of the Cartesian coordinate. P expresses the mean pressure, ρ the density and ν the kinematic viscosity.

The well-known k-ε turbulence model is employed in order to simulate the turbulent flow around the submarine precisely. This turbulence model is applicable when there are not high pressure changes along the hull and separation near the hull. In this case, k-ε turbulence model is used because the vessel is fully submerged and hence there are no free surface effects. During the analyses, Reynolds stress tensor is calculated as follow;

$$\overline{\mathrm{u_i' u_j'}} = -\nu_\mathrm{t}\left(\frac{\partial \mathrm{U_i}}{\partial \mathrm{x_j}} + \frac{\partial \mathrm{U_j}}{\partial \mathrm{x_i}}\right) + \frac{2}{3}\delta_{\mathrm{ij}}\mathrm{k} \tag{4}$$

Here, ν_t is the eddy viscosity and expressed as an empirical constant ($C_\mu = 0.09$). k is the turbulent kinetic energy and ε is the turbulent dissipation rate. In addition to the continuity and momentum equations, two transport equations are solved for k and ε:

$$\frac{\partial k}{\partial t}+\frac{\partial\left(kU_j\right)}{\partial x_j}=\frac{\partial}{\partial x_j}\left[\left(\nu+\frac{\nu_t}{\sigma_k}\right)\frac{\partial k}{\partial x_j}\right]+P_k-\varepsilon \quad (5)$$

$$\frac{\partial \varepsilon}{\partial t}+\frac{\partial\left(kU_j\right)}{\partial x_j}=\frac{\partial}{\partial x_j}\left[\left(\nu+\frac{\nu_t}{\sigma_\varepsilon}\right)\frac{\partial \varepsilon}{\partial x_j}\right]+C_{\varepsilon 1}P_k\frac{\varepsilon}{k}-C_{\varepsilon 2}\frac{\varepsilon^2}{k} \quad (6)$$

$$P_k=-\overline{u_i'u_j'}\frac{\partial U_i}{\partial x_j} \quad (7)$$

where, $C_{\varepsilon 1}=1.44$, $C_{\varepsilon 2}=1.92$ turbulent Prandtl numbers for k and ε are $\sigma_k=1.0$ and $\sigma_\varepsilon=1.3$, respectively. Further explanations for the k-ε turbulence model may be found in (Wilcox 2006).

2.2 *Uncertainty Assessment*

In this study, uncertainty analysis has been made via Grid Convergence Method as recommended in the ITTC procedure for CFD verification (ITTC 2011a). This method firstly was proposed by Roache and then improved with different studies (Roache 1998). The procedure implemented in this study has been explained below (Celik et al. 2008).

Let h_1, h_2 and h_3 are grid lengths and $h_1 < h_2 < h_3$. The refinement factors (r) are as follows:

$$r_{21}=\frac{h_2}{h_1} \qquad r_{32}=\frac{h_3}{h_2} \quad (8)$$

Refinement factors should be greater than 1.3 in accordance with the experiments (Roache 1998). Grid lengths' refinement is selected as a value of $\sqrt{2}$. Because of the mesh algorithm, number of cells (N) has been taken into account during the calculation of the refinement factors. This choice is crucial in uncertainty analyses especially for unstructured mesh system. Therefore, these values have been differentiated.

$$r_{21}=\left(\frac{N_1}{N_2}\right)^{1/3} \qquad r_{32}=\left(\frac{N_2}{N_3}\right)^{1/3} \quad (9)$$

The differences (ε) between generated cell numbers can be calculated below:

$$\varepsilon_{21}=X_2-X_1 \qquad \varepsilon_{32}=X_3-X_2 \quad (10)$$

Here, X is the solution of the analysis.

At this point, convergence condition R can be examined.

$$R=\frac{\varepsilon_{21}}{\varepsilon_{32}} \quad (11)$$

In this study, R is calculated between 0 and 1 which means that the solution is converged monotonically. Detailed information about Grid Convergence Index (GCI) can be found in (Roache 1998).

3 COMPUTATIONAL METHOD

3.1 *Grid Structure and Boundary Conditions*

A proper computational domain has been created in order to simulate the flow around the submarine model with/without self-propulsion. Three dimensional grids have been employed for modelling the flow region with fully hexahedral elements.

Figure 1 shows the computational domain with the assigned boundary conditions on the surfaces. The left side of the computational domain is defined as velocity inlet and the right side is defined as pressure outlet. The submarine surface is considered as no-slip wall. In addition, the side surfaces are also defined as symmetry. More detailed information on boundary conditions can be obtained from the theory guide of the commercial CFD software (Star CCM+ 2015).

The computational domain is divided into three dimensional finite volumes and discretized according to the finite volume method (FVM). The main dimensions of the computational domain are determined in accordance with the ITTC guidelines to properly determine the flow (ITTC 2011b). To create a computational domain, unstructured hexahedral elements are employed in the whole domain. The mesh refinements are also made in the bow, stern and the wake area of the form. Unstructured mesh of the computational domain is given in Fig. 2. For propulsion analyses including open water and self-propelled cases; polyhedral mesh structure has been employed but also a fine mesh region has been created around the propeller disc in order to model the interaction of the hull and the propeller more accurately.

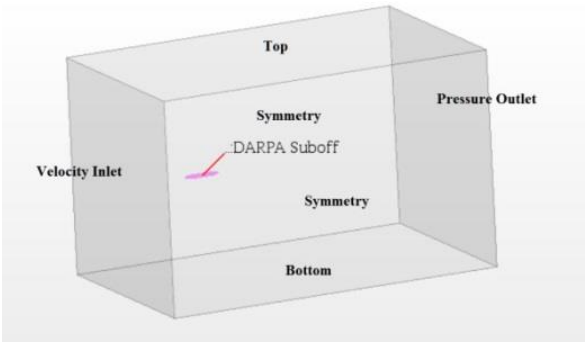

Figure 1. Computational domain and the boundary conditions.

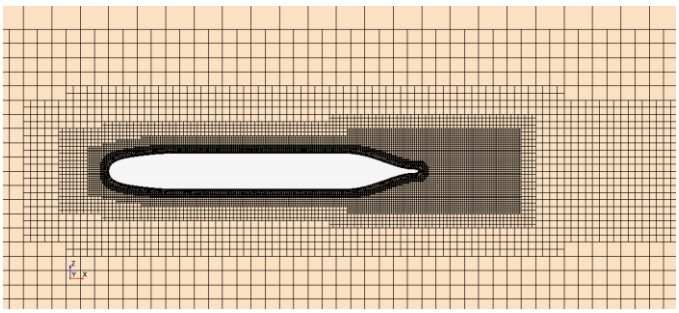

Figure 2. Unstructured mesh of the computational domain.

3.2 *Solution Strategy*

k-ε turbulence model is used in the computational analyses because there are no high pressure gradients along the hull. In other words, the slenderness of the hull geometry makes the effect of boundary layer separations on the flow characteristics around the hull insignificant.

The pressure field is solved by using SIMPLE algorithm which is based on pressure-velocity coupling. SIMPLE is a commonly used algorithm for calculating pressure and velocity fields in an iterative manner. Especially for steady state analyses, it reduces the computational time rapidly (Versteeg et al. 2007). All the governing equations are discretized using a cell based finite volume method and the advection terms are discretized with a first-order upwind interpolation scheme.

Because of the flow characteristics, the analyses have been made via single phase assumption. Free surface effects are not taken into account in either resistance or propulsion analyses. Viscous effects near the ship are taken into account by modelling the boundary layer with an appropriate grid structure keeping y+ values of the hull in a reasonable range (30-300).

For self-propulsion analyses based on body force method, an actuator disc has been modeled using actuator disc theorem. Distribution of body forces has been applied in this actuator disc region. Here, actuator disc region represents an infinite-bladed propeller. So the characteristics of hydrodynamic performance of model propeller have been defined in the region. The actuator disc and the model propeller have the same diameter and identical distributions of elemental thrust along the radius (Krasilnikov 2013).

Also, self-propulsion analyses have been done using Moving Reference Frame (MRF) technique. Within this technique, a rotating region has been created behind the submarine including the model propeller itself. According to this technique, the governing equations are transformed into a rotating frame to get a steady-state solution (Moussa 2014).

4 VERIFICATION AND VALIDATION

In this section, five different grid sizes have been used as given in Table 1 for bare hull resistance analyses. In order to determine the uncertainty, three groups are created including three mesh cases. Different cell numbers have been used for modelling the computational domain for resistance analyses. After verification and validation, the optimum cell number has been chosen for the rest of the analyses including actuator disc and self-propulsion cases for different velocities.

Table 2 shows that the convergence condition R is between 0 and 1 as described in Section 2.2. As explained above, analysis groups are selected as 1-2-3, 2-3-4 and 3-4-5. The results of uncertainty analyses are shown below in Table 3.

The numerical results are also compared with the experimental results in order to validate the numerical method as given in Table 4. The numerical result is of the optimum mesh number. The uncertainty analyses have been made for total ship resistance analyses. Fine mesh algorithm has been chosen as the optimum one for resistance analyses. The finer mesh may not lead to more accurate results.

Table 1. Total resistance via different cell numbers.

		Bare Hull Resistance	
#	Name	Number of Cells	Resistance (N)
1	Finer	937.000	88.17
2	Fine	516.154	88.41
3	Medium	276.000	89.21
4	Coarse	175.659	90.93
5	Coarser	103.068	95.90

Table 2. Convergence conditions for uncertainty analyses.

Analysis Set	R
1 2 3	0.300
2 3 4	0.465
3 4 5	0.346

Table 3. Uncertainty analyses for bare hull resistance.

	Bare Hull Resistance
Analysis Set	% GCI_{FINE}
1 2 3	0.15
2 3 4	0.75
3 4 5	1.41

Table 4. Validation of the numerical method.

V_s (m/s)	$R_{T\text{-}EXP}$ (N)	$R_{T\text{-}CFD}$ (N)	Absolute Relative Difference (%)
3.046	87.4	88.41	1.15

Attention has been paid in order to validate the numerical method with the experiments in addition to the uncertainty analysis of the method for verification and validation process. The optimum cell number has been determined and also validated with the available experimental data. The free stream velocity has been considered as 3.046 m/s for bare hull conditions during the uncertainty analyses. The number two (#2) mesh structure (fine) has been selected for the rest of the analyses.

5 COMPUTATIONAL RESULTS AND DISCUSSIONS

This section focuses on the computational results of the flow simulation around DARPA Suboff geometry for bare hull condition using the optimum cell number determined with verification and validation process above. In addition, open water flow analyses for E1619 propeller have been performed. Following the resistance and open water analyses, self-propulsion tests have been done via body force propeller method. For this purpose, the open water propeller results have been coupled with RANSE solver by creating an actuator disc representing the finite-bladed model propeller. Then, the self-propulsion point has been determined for one velocity. This method has been discussed in terms of thrust, torque, wake fraction factor, thrust deduction factor, delivered power and thrust power. The advantageous and disadvantageous properties of these methods have been highlighted.

5.1 *Geometrical Dimensions*

DARPA Suboff submarine model is a widely used benchmark form. Table 5 shows the main particulars of the model submarine. Also 3-D model of the submarine bare hull can be seen in Figure 3.

Table 5. Main particulars of DARPA Suboff (AFF-1)

L_{OA} (m)	4.356
L_{BP} (m)	4.261
D_{max} (m)	0.508
S (m^2)	5.980
∇ (m^3)	0.717

Figure 3. 3-D view of DARPA Suboff bare hull

Table 6 on the other hand gives the main particulars of the model propeller E1619 used in the self-propulsion analyses. 3-D model of the model propeller can be found in Figure 4.

Table 6. Main particulars of E1619 propeller.

	Open Water	Self-Propulsion
D (m)	0.485	0.262
P/D at 0.7R	1.15	1.15
Z	7	7
A_E/A_0	0.608	0.608

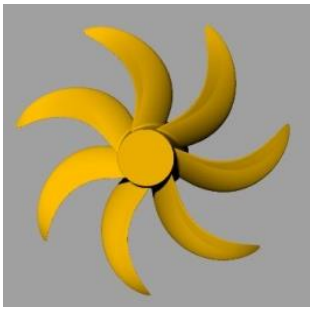

Figure 4. 3-D view of E1619 model propeller

5.2 *Computational Results*

A series of analyses has been conducted for prediction of total resistance of DARPA Suboff bare hull. One may see from Table 7 that the numerical method can calculate the submarine total resistance with an acceptable error when compared with the experiments.

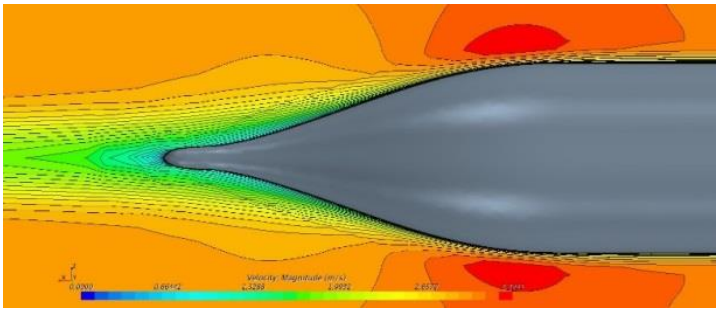

Figure 5. Velocity contours on the aft body of the submarine.

Figure 5 shows the velocity contours around the aft body of the submarine. It can be seen that there is no separation near the hull surface.

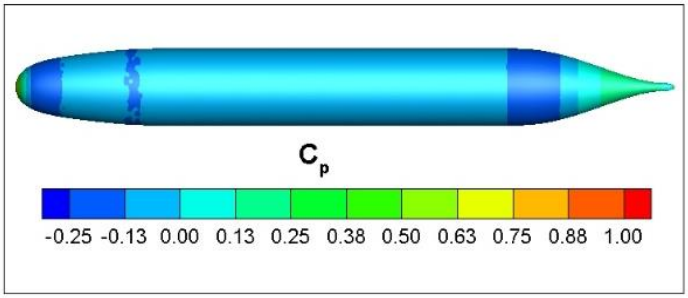

Figure 6. Non-dimensional pressure distribution on the submarine surface.

Figure 6 shows the non-dimensional pressure distribution on the submarine surface. The pressure is higher on the aft and fore body as expected.

Figure 7 shows the non-dimensional pressure distribution on the propeller blades in open water condition. Figure 8 presents the non-dimensional pressure distribution on the propeller blades behind the submarine.

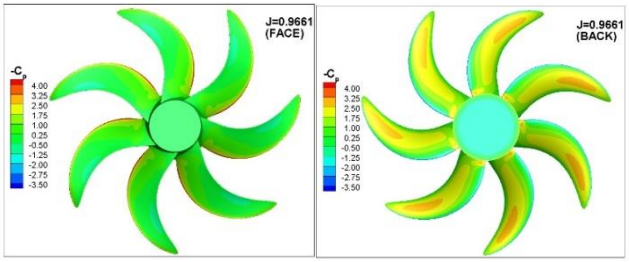

Figure 7. Non-dimensional pressure distribution on the propeller blades in open water condition.

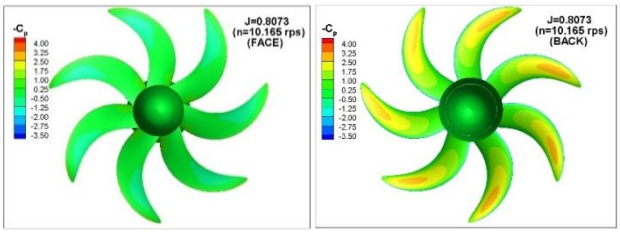

Figure 8. Non-dimensional pressure distribution on the propeller blades behind the submarine.

Table 7. Comparison of the numerical and experimental results.

Rn * 10^6	V (m/s)	$R_{T\text{-}EXP}$ (N)	$R_{T\text{-}CFD}$ (N)	Absolute Relative Difference (%)
12.40	3.046	87.4	88.41	1.15
20.95	5.144	242.2	234.91	3.01
24.81	6.091	332.9	321.96	3.28
29.17	7.161	451.5	435.41	3.56
33.54	8.231	576.9	564.62	2.13
37.69	9.255	697	702.91	0.84

Figure 9 shows the comparison of open water propeller characteristics for numerical and experimental methods. The results are quite satisfactory in a wide range of advance ratios.

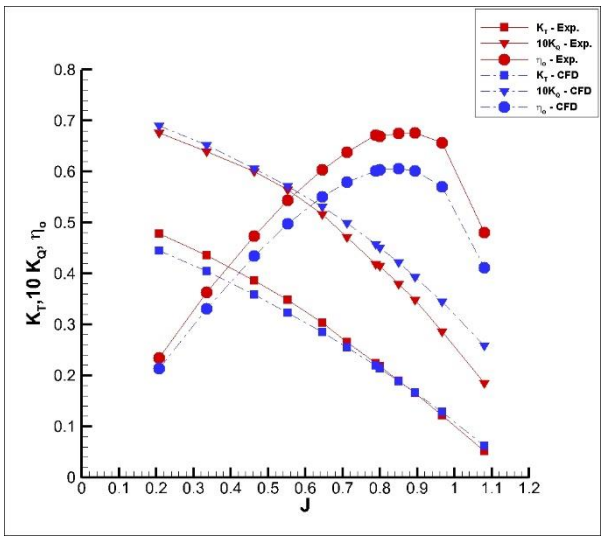

Figure 9. Comparison of thrust, torque and efficiency of E1619 propeller.

Figures 10 and 11 show the computed self-propulsion point for DARPA Suboff bare hull at a constant velocity of 3.046 m/s.

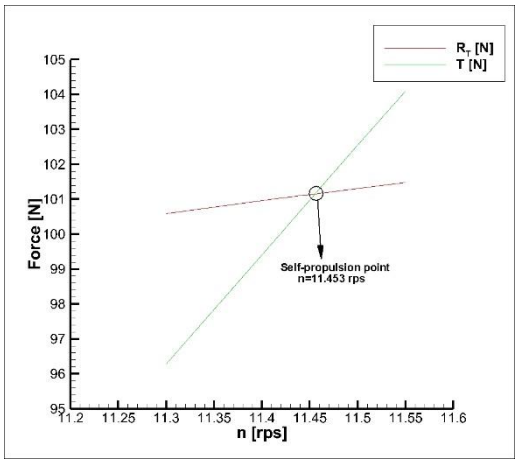

Figure 10. Self-propulsion point of DARPA Suboff with actuator disc theory.

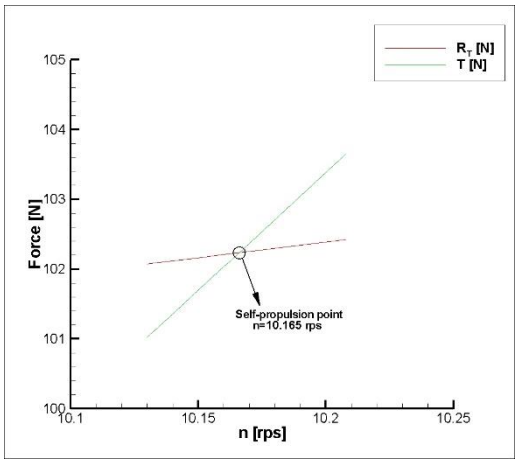

Figure 11. Self-propulsion point of DARPA Suboff in the presence of E1619 propeller.

It can be said that the actuator disc theory gives slightly higher self-propulsion point for the submarine when compared with the other technique having the actual propeller model behind the submarine. Later the nominal wake coefficient, thrust deduction factor, hull efficiency, relative rotative efficiency, open water propeller efficiency and propulsion efficiency have been determined using the following equations. Finally, effective power and delivered power have been calculated by both techniques.

The propulsion performance of a bare form is briefly described as below (ITTC 1978).

The nominal wake coefficient here is calculated as follow:

$$w = 1 - \frac{V_A}{V_S} \tag{12}$$

Here, V_A is the average flow velocity in the propeller plane, V_S is the incoming flow velocity towards the hull. V_A is calculated by

$$J = \frac{V_A}{n \cdot D} \tag{13}$$

Here J is advance coefficient, D is propeller diameter and n is propeller rotation speed. The thrust deduction factor on the other hand can be calculated by

$$t = 1 - \frac{R_T}{T} \quad (14)$$

where, T is thrust force. The hull efficiency is expressed as the ratio of effective power to propeller thrust power. It can be expressed as follows:

$$\eta_H = \frac{1-t}{1-w} \quad (15)$$

The relative rotation efficiency is expressed as the ratio of the open water propeller torque to the torque of the propeller working behind the hull.

$$\eta_R = \frac{Q_o}{Q} \quad (16)$$

The open water propeller efficiency at V_A is calculated by the help of the following equation. This efficiency is calculated from open water data in momentum theory.

$$\eta_o = \frac{T \cdot V_A}{2\pi \cdot n \cdot Q_o} \quad (17)$$

The propulsion efficiency is then expressed as follows:

$$\eta_D = \eta_H \cdot \eta_o \cdot \eta_R \quad (18)$$

Effective power is the power required to pull the hull at constant speed (V_S).

$$P_E = R_T \cdot V_S \quad (19)$$

The power delivered to the propeller is calculated as follow:

$$P_D = \frac{P_E}{\eta_D} \quad (20)$$

Thrust loading factor in momentum theory can be calculated as below:

$$C_{T_h} = \frac{T}{\rho \cdot V_A{}^2 \cdot D^2 \cdot \frac{\pi}{8}} \quad (21)$$

The ideal efficiency of propeller in momentum theory is expressed as below (Bertram 2012):

$$\eta_i = \frac{2}{1+\sqrt{1+C_{T_h}}} \quad (22)$$

Table 8 shows the self-propulsion characteristics of DARPA Suboff with E1619 model propeller. During the calculations, thrust identity method has been used. By this method, non-dimensional thrust coefficient has been derived from the propeller thrust. Then, advance ratio of the propeller has been calculated using thrust coefficient in open water performance curve of the propeller. Finally, average inflow velocity coming to the propeller has been gained using advance ratio.

Table 8. The self-propulsion characteristics of DARPA Suboff with two methods.

	Actuator Disc	Model Propeller
V_S (m/s)	3.046	3.046
V_A (m/s)	2.690	2.169
J	0.896	0.815
n (rps)	11.453	10.165
R_T (N)	101.0708	102.1987
T (N)	101.0708	102.1987
Q (Nm)	5.5906	5.5357
Q_0 (Nm)	5.574	5.148
$w_{nominal}$	0.32	0.32
t	0.125	0.135
η_H	0.991	1.215
η_R	0.997	0.930
η_o	0.678	0.674
η_D	0.669	0.762
η_i	0.919	-
P_E (W)	269.297	269.297
P_D (W)	402.307	353.557

6 CONCLUSIONS

In this study, the bare hull resistance of DARPA Suboff form has been investigated using CFD based finite volume method. A verification and validation assessment has been done. After selecting the optimum mesh number, total resistance of the submarine has been calculated for different velocities and compared with the experimental results. In addition, open water flow analyses for E1619 model propeller have been carried out. Again, the results have been validated with available experimental data. Following the resistance and open water analyses of model propeller, self-propulsion analyses have been done using both the actuator disc theory and modeling the actual propeller itself behind the submarine. The self-propulsion characteristics of DARPA Suboff have then been determined for a constant velocity. It is found that CFD method is robust for prediction of self-propulsion point of underwater vehicles. Because prediction of self-propulsion point of an underwater vehicle is possible numerically without any need to complicated and expensive experimental methods. Moreover it is obtained that the actuator disc theory gives a slightly higher self-propulsion

point while the total resistance is lower since there is no propeller behind the hull. Actuator disc theory has higher delivered power when compared with the model propeller technique. In the presence of the propeller, total resistance is higher, so the thrust deduction also increases. So one may say that the actuator disc theory can be applied safely in self-propulsion point estimation. Actuator disc theory may be suitable for prediction of self-propulsion characteristics such as delivered power.

The main highlight of this paper is that self-propulsion tests with CFD method using different techniques may be effective for preliminary design stage for obtaining fast results.

As a future work, self-propulsion calculations will be done using an average advance coefficient gained from thrust and torque identity methods.

NOMENCLATURE

U_i	mean velocity
u_i'	fluctuation velocity component
P	mean pressure
ρ	fluid density
k	turbulent kinetic energy
ε	turbulent dissipation rate
R_T	ship total resistance
L_{OA}	length overall
L_{BP}	length between perpendiculars
D_{max}	submarine maximum diameter
S	submarine wetted surface area
∇	submarine displacement
D	propeller diameter
P/D	propeller pitch ratio
Z	number of blades
A_E/A_0	propeller blade expansion ratio
w	nominal wake coefficient
V_A	the mean flow velocity at the propeller plane
V_S	incoming flow velocity
n	propeller rotation speed
J	advance ratio
t	thrust deduction factor
T	propeller thrust force
η_H	hull efficiency
η_R	relative rotation efficiency
η_o	open water propeller efficiency
η_D	propulsion efficiency
P_E	effective power
P_D	delivered power
C_{T_h}	thrust loading factor
η_i	ideal efficiency of the propeller

ACKNOWLEDGEMENTS

We would like to thank Mr. Emre Kahramanoglu for his valuable support in uncertainty assessment throughout this study.

REFERENCES

Vaz G., Toxopeus S., and Holmes S. 2010. Calculation of Maneuvering Forces on Submarines using Two Viscous-Flow Solvers. *Proceedings of the ASME 2010 29th International Conference on Ocean, Offshore and Arctic Engineering Shanghai, China.*

Zhang, N. and Zhang, S. 2014. Numerical simulation of hull/propeller interaction of submarine in submergence and near surface conditions, *J. Hydrodyn. Ser B, vol. 26, no. 1, pp. 50–56.*

Berger, S., Druckenbrod, M., Greve, M., Abdel-Maksoud, M. and Greitsch, L. 2011. An Efficient Method for the Investigation of Propeller Hull Interaction. *14th Numerical Towing Tank Symposium.*

Rijpkema, D., Starke, B. and Bosschers, J. 2013. Numerical simulation of propeller-hull interaction and determination of the effective wake field using a hybrid RANS-BEM approach. *Third International Symposium on Marine Propulsors, Launceston, Tasmania, Australia.*

Ozdemir, Y. H., Cosgun, T., Dogrul, A., Barlas, B. 2016. A numerical application to predict the resistance and wave pattern of KRISO container ship. *Brodogradnja, vol. 67, no. 2, 47-65.*

Seo, J. H., Seol, D. M., Lee, J. H., and Rhee, S. H. 2010. Flexible CFD meshing strategy for prediction of ship resistance and propulsion performance. *Int. J. Nav. Archit. Ocean Eng., vol. 2, no. 3, pp. 139–145.*

Villa, D. and Brizzolara, S. 2012. Ship Self Propulsion with different CFD methods: from actuator disc to viscous inviscid unsteady coupled solvers. *10th International Conference on Hydrodynamics, St. Petersburg, Russia.*

Kinaci, O. K., Kukner, A., and Bal, S. 2013. On Propeller Performance of DTC Post-Panamax Container Ship. *International Journal of Ocean System Engineering, 3(2), 77-89.*

Kinaci, O.K., Sukas, O.F. and Bal, S. 2016. Prediction of Wave Resistance by a RANSE based CFD Approach. *Proceedings of the Institution of Mechanical Engineers, Part M, Journal of Engineering for the Maritime Environment, Vol. 230, Issue 3, pp: 531-548.*

Carrica, P. M., Castro, A. M. and Stern, F. 2010. Self-propulsion computations using a speed controller and a discretized propeller with dynamic overset grids. *J. Mar. Sci. Technol., vol. 15, no. 4, pp. 316–330.*

Chase, N. 2012. Simulations of the DARPA Suboff submarine including self-propulsion with the E1619 propeller. *Master Thesis, University of Iowa.*

Chase, N. and Carrica, P. M. 2013. Submarine propeller computations and application to self-propulsion of DARPA Suboff. *Ocean Eng., vol. 60, pp. 68–80.*

Budak, G. and Beji, S. 2016. Computational Resistance Analyses of a Generic Submarine Hull Form and Its Geometric Variants. *J. Ocean Technology, 11, pp. 77-86.*

Delen, C., Sezen, S., and Bal, S. 2017. Computational investigation of self-propulsion performance of DARPA Suboff vehicle. *Tamap Journal of Engineering, vol. 1, no. 4.*

Wilcox, D. C. 2006. Turbulence Modeling for CFD. *3rd edition. La Cãnada, Calif.: D C W Industries.*

ITTC 2011a. 7.5-03-01-04 CFD, General CFD Verification. *ITTC - Recommended Procedures and Guidelines.*

Roache, P. J. 1998. Verification of Codes and Calculations. *AIAA J., vol. 36, no. 5, pp. 696–702.*

Celik, I. B., Ghia, U. and Roache, P. J. 2008. Procedure for estimation and reporting of uncertainty due to discretization in CFD applications. *J. Fluids Eng.-Trans. ASME, vol. 130, no. 7.*

CD-adapco 2015. *Star CCM+ Documentation.*

ITTC 2011b. "Practical guidelines for ship CFD applications," Proceedings of 26th ITTC, Rio de Janeiro.

Versteeg, H. and Malalasekera, W. 2007. An Introduction to Computational Fluid Dynamics: The Finite Volume Method, 2nd edition. *Harlow, England; New York: Prentice Hall.*

Krasilnikov, V. 2013. Self-Propulsion RANS Computations with a Single-Screw Container Ship. *Third International Symposium on Marine Propulsors, Tasmania, Australia.*

Moussa, K. 2014. Computational Modeling of Propeller Noise: NASA SR-7A Propeller. *Master Thesis, University of Waterloo, Waterloo, Ontario, Canada.*

ITTC 1978. Report of Performance Committee. *Proceedings of 15th ITTC, Hague.*

Bertram, V. 2012. Practical Ship Hydrodynamics, 2nd edition. Elsevier.